Investigation of discrete states and quasidiscrete structures observed in ^{150}Sm and ^{152}Sm using the $(p,t\gamma)$ reaction

P. Humby,[1,2] A. Simon,[1,3] C. W. Beausang,[1] J. M. Allmond,[4] J. T. Harke,[5] R. J. Casperson,[5] R. Chyzh,[6] M. Dag,[6] K. Gell,[1] R. O. Hughes,[5] J. Koglin,[5] E. McCleskey,[6] M. McCleskey,[6] S. Ota,[5] T. J. Ross,[7] A. Saastamoinen,[6] T. Tarlow,[1] and G. Vyas[1]
[1]*Department of Physics, University of Richmond, Richmond, Virginia 23171, USA*
[2]*Department of Physics, University of Surrey, Surrey, GU27XH, United Kingdom*
[3]*Department of Physics, University of Notre Dame, Notre Dame, Indiana 46556*
[4]*Physics Division, Oak Ridge National Laboratory, Oak Ridge, Tennessee 37831, USA*
[5]*Lawrence Livermore National Laboratory, Livermore, California 94551, USA*
[6]*Cyclotron Institute, Texas A&M University, College Station, Texas 77843, USA*
[7]*Department of Chemistry, University of Kentucky, Lexington, Kentucky 40506, USA*
(Received 19 September 2016; published 14 December 2016)

New levels and γ-ray transitions were identified in ^{150,152}Sm utilizing the (p,t) reaction and particle-γ coincidence data. A large, peak-like structure observed between 2.3–3.0 MeV in excitation energy in the triton energy spectra was also investigated. The orbital angular-momentum transfer was probed by comparing the experimental angular distributions of the outgoing tritons to calculated distorted wave Born approximation curves. The angular distributions of the outgoing tritons populating the peak-like structure are remarkably similar in the two reactions and are significantly different from the angular distributions associated with the nearby continuum region. Relative partial cross sections for the observed levels, angle averaged between 34 and 58 degrees, were measured. In ^{150}Sm, 39(4)% of the strength of the peak-like structure could be accounted for by the observed discrete states. This compares with a value of 93(15)% for ^{152}Sm.

DOI: 10.1103/PhysRevC.94.064314

I. INTRODUCTION

The samarium ($Z = 62$) isotopes near $N = 90$ lie in a region of rapid shape change from spherical to deformed with increasing neutron number. This has led to this region of the nuclear chart being the focus of intense experimental and theoretical study; see, for example, Refs. [1–6]. In the early two-neutron-transfer experiments by Maxwell [7] and Bjerregaard [8], excited $J^\pi = 0^+$ states were observed to have large cross sections relative to the ground state in the ^{152}Sm(p,t) and ^{150}Sm(t,p) reactions. This was interpreted in terms of shape coexistence [7,8] and the rapid onset of deformation, inviting further interest in these nuclei. In general, the $N = 90$ region provides a rich testing ground for models that attempt to describe transitional and deformed nuclei.

Two-neutron-transfer reactions provide an excellent tool with which to study both the removal of pairs of correlated neutrons from valence orbitals, typically populating states at relatively low excitation energies, as well as the removal of neutrons from deep below the Fermi surface. Following the work of Maxwell [7], further Sm(p,t) experiments were performed with improved energy resolution for the outgoing tritons (see, for example, Refs. [9–12]) at various incident proton beam energies. In the 1981 study by Struble *et al.* [13] a large, broad enhancement of two-neutron-transfer strength at an excitation energy of approximately 6 MeV was observed in the ^{148,150,152,154}Sm(p,t) reactions. An additional, much narrower, peak-like structure at an excitation energy of 2.2–3.1 MeV was observed in both the ^{152,154}Sm(p,t) reactions. In the ^{158}Gd$(p,t)^{156}$Gd study by Riezebos *et al.* [14] a rapid increase in 2^+, 4^+, and 6^+ strength was observed above 2 MeV in excitation energy. An interesting lack of monopole strength was reported above this energy, providing motivation to study the L-transfer distribution at this excitation energy in nearby nuclei.

In the present work, the peak-like structure (PLS) is studied in detail and ^{150,152}Sm are studied for the first time using the $(p,t\gamma)$ coincidence technique. The coincident detection of the γ ray allows for excellent selectivity and sensitivity and allows us to identify multiple new levels and γ-ray transitions in each nucleus. Triton angular distributions, selected by specific γ-ray transitions, probe the angular-momentum transfer to both low-lying discrete states and states in the PLS and are compared with calculated distorted wave Born approximation (DWBA) curves.

II. EXPERIMENTAL ARRANGEMENT

A 25 MeV proton beam from the K-150 cyclotron at the Cyclotron Institute of Texas A&M University was incident upon isotopically enriched ^{152}Sm and ^{154}Sm targets of 98% and 99% purity, respectively, and approximately 1 mg/cm^2 thickness. The ^{152}Sm target was bombarded for 42 h and the ^{154}Sm target for 35 h with average beam currents of 1.4 and 1.2 nA, respectively.

The outgoing light ions and γ rays were detected by using the STARLiTeR array, which uses the same configuration as that described in detail in Ref. [15]. This array consisted of the Silicon Telescope Array for Reaction Studies (STARS) ΔE-E silicon telescope and the Livermore Texas Richmond (LiTeR) array of bismuth-germanate-shielded (BGO-shielded) high-purity Ge (HPGe) clover detectors providing particle-γ and particle-γ-γ coincidence capability. A total of 1.5×10^5

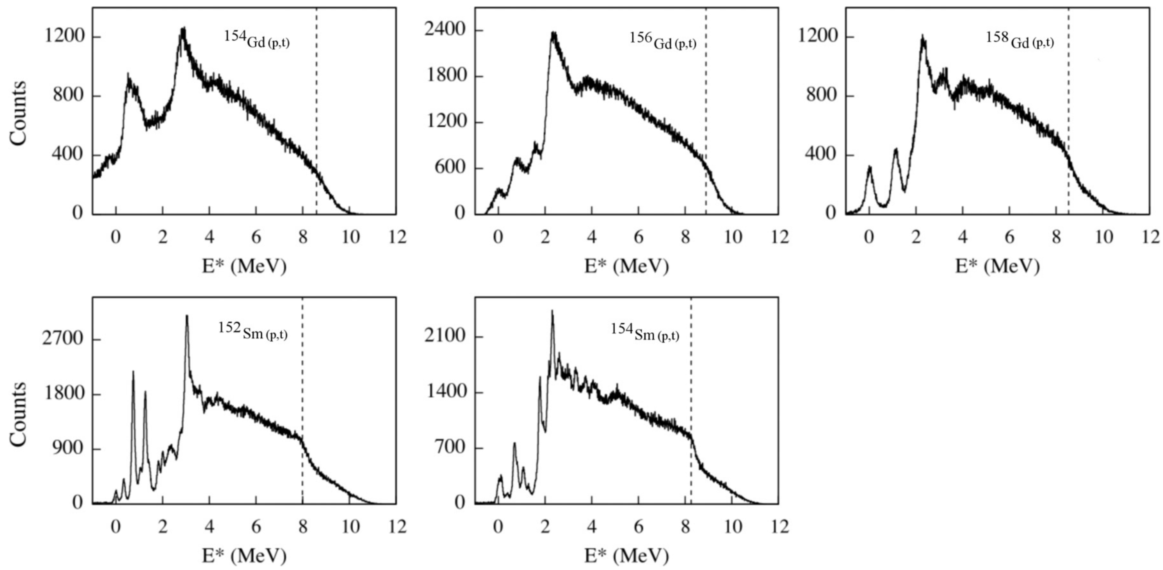

FIG. 1. Triton projections of the (t,γ) matrices produced in the ^{154,156,158}Gd(p,t) and ^{152,154}Sm(p,t) reactions. The single-neutron separation energies are indicated by the dashed lines. The Gd data are from Refs. [18,19]. It can be seen that the energy resolution is much improved in the Sm data.

t-γ-γ coincidences were observed for the ^{152}Sm(p,t) reaction and 1.4×10^5 for the ^{154}Sm(p,t) reaction, allowing t-γ-γ measurements for only the strongest transitions. STARS consisted of a 0.14-mm-thick ΔE detector and a 1-mm-thick E detector, both segmented into 24 rings (θ) and 8 sectors (ϕ). The distance between the target foil and the ΔE detector was 18 mm. The angular coverage of the telescope was 34 to 58 degrees. An aluminum δ shield was placed between the target position and STARS to shield the ΔE detector from secondary electrons. An aluminum tunnel passed through the center of the telescope to shield the inner rings from scattered beam particles. The six HPGe clover detectors were positioned in pairs at angles of 47°, 90°, and 133° with respect to the incident proton beam at a distance of 13 cm from the target position.

The Si telescope was calibrated by using a ^{226}Ra source which provides α particles at energies of 4.6, 4.8, 5.3, 5.5, 6.0, and 7.7 MeV. An additional nine calibration points between 4.4 and 16.1 MeV were obtained by using levels populated in the ^{12}C(p,p') reaction. Well-known levels at low excitation energy populated in the ^{152,154}Sm(p,t) reactions as well as the onset of the ^{152,154}Sm(p,tn) channels at the neutron separation energies of 7.9867(4) and 8.2577(6) MeV [16], respectively, were also used. Energy deposited in adjacent rings of the Si detectors was summed and induced noise in neighboring rings was corrected for. The energy losses due to the Al and Au dead layers of the Si detectors were calculated by using the Energy Loss And Straggling Tool (ELAST) program [17] and the recoil energy imparted to the target nucleus was also accounted for. A resolution (full width at half maximum, FWHM) of 130 keV was obtained for the ground state of ^{150}Sm in the ^{152}Sm(p,t) reaction.

The HPGe clover detectors were calibrated using ^{22}Na, ^{54}Mn, ^{57}Co, ^{60}Co, ^{109}Cd, ^{133}Ba, ^{137}Cs, and ^{152}Eu sources. The photopeak efficiency was 4.8% at 103 keV and an energy resolution of 2.6 and 3.5 keV (FWHM) was obtained at energies of 122 and 963 keV, respectively.

III. TRITON PROJECTIONS AND IDENTIFICATION OF DISCRETE STATES

Energy spectra for tritons in coincidence with γ rays from the recent ^{154,156,158}Gd(p,t) studies by Ross *et al.* [18] and Allmond *et al.* [19] are shown in Fig. 1 and compared with those obtained in the present work for the ^{152,154}Sm(p,t) reactions. The PLS is clearly present between 2.1–3.3 MeV excitation energy in all of these reactions. The excitation energy of the structure is plotted in Fig. 2 and appears to decrease with increasing neutron number.

Particle-γ coincidences are a powerful spectroscopic tool; see, for example, Ref. [20]. A gate placed on a triton energy of

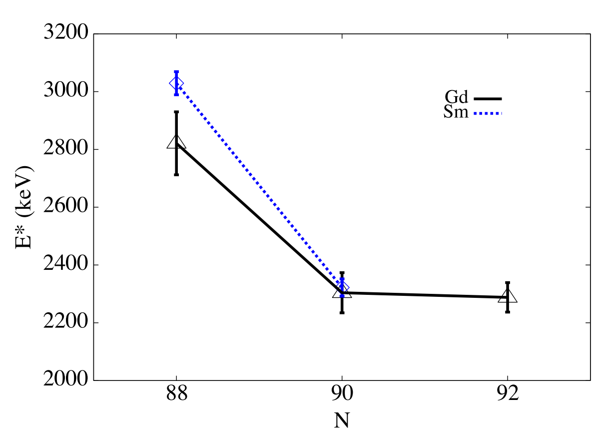

FIG. 2. The excitation energy of the PLS as a function of neutron number for the Gd (black points and solid black line) and Sm (blue points and dashed blue line) isotopes.

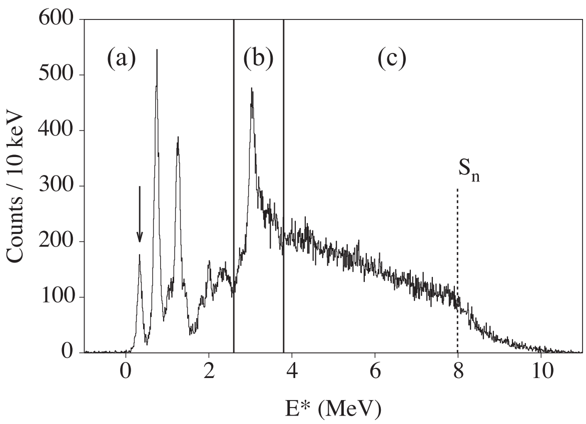

FIG. 3. Triton energy spectrum in coincidence with the 334 keV γ-ray transition between the first 2^+ state in ^{150}Sm and the ground state. The triton peak corresponding to direct population of the level is indicated by the arrow. In part (a), peaks corresponding to discrete states can be seen. In part (b), at intermediate excitation energy, the PLS is present. In part (c), the smoothly varying continuum region and the onset of the (p,tn) channel above the single-neutron separation energy can be observed.

interest in the t-γ coincidence matrix corresponds to gating on a certain excitation energy in the residual nucleus. This gate returns a spectrum of γ rays that must be emitted from states at or below this excitation energy and often enhances low-intensity γ rays that are obscured in the total projection. On the other hand, gating on a γ ray in the t-γ matrix typically gives a triton energy spectrum with a discrete peak corresponding to the direct population of the γ-ray emitting level, as well as counts at higher excitation energy which correspond to states that feed that level, both directly and indirectly. These features can be observed in the spectrum shown in Fig. 3 obtained with a gate placed on the 334 keV γ ray from the transition between the first 2^+ state in ^{150}Sm and the ground state. The peak at 334 keV corresponds to direct population of the 2^+ level. Also visible are the plethora of other discrete states that are directly populated by the (p,t) reaction and then feed the 2^+ state as well as a smooth continuum region above approximately 3.5 MeV. A further example is shown in Fig. 4. In Fig. 4(a), a γ-ray energy spectrum showing a section of the total γ-ray projection from the ^{152}Sm$(p,t\gamma)$ coincidence matrix is shown. Figure 4(b) shows a γ-ray energy spectrum in coincidence with tritons corresponding to an excitation energy range of 1210–1290 keV in ^{150}Sm. The 922 keV γ ray is from the level at 1255 keV. The 712 keV transition is from the level at 1046 keV, which is fed by the 1255 keV level via a 209 keV transition not shown in the figure. Figure 4(c) shows a triton energy spectrum in coincidence with the 922 keV γ ray. This spectrum, typical of those observed when gating on nonyrast levels, shows the direct population peak at 1255 keV and very little feeding from higher-lying excited states.

To identify new discrete states in ^{150,152}Sm, a gate is first placed on a γ ray of interest in the t-γ matrix. The approximate excitation energy of the level (typical accuracy of ~20–30 keV) is then measured by fitting the energy of the triton peak (see Fig. 4), corresponding to direct population of the level. Subtracting the γ-ray energy from the excitation energy corresponding to the triton peak often identifies the level that is being fed by the transition. This can only be performed unambiguously either when there is just one possible final level within the experimental uncertainty, when multiple γ rays depopulate the level, or when the γ-ray placement can be confirmed by using t-γ-γ coincidences. Once the γ ray has been placed in the level scheme, the γ-ray energy can be summed with the energy of the level that is being fed, which provides a much more precise measurement (typically 0.2 keV) of the excitation energy of the state of interest; see Ref. [20] for more details.

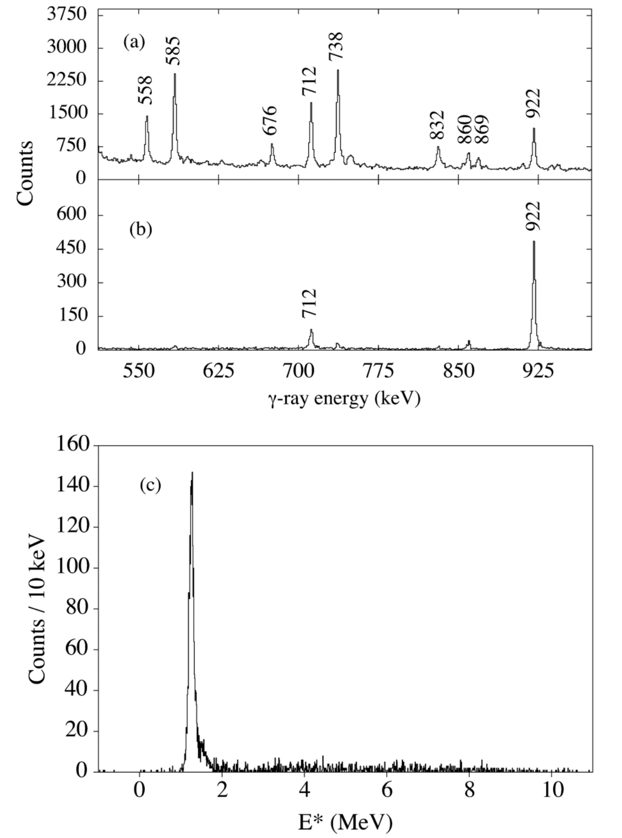

FIG. 4. (a) A γ-ray energy spectrum showing a section of the total γ-ray projection from the ^{152}Sm$(p,t\gamma)$ coincidence matrix. (b) The γ-ray energy spectrum in coincidence with tritons corresponding to an excitation energy between 1210 and 1290 keV. The 922 keV γ ray is from the level at 1255 keV in ^{150}Sm. The 712 keV γ is from the level at 1046 keV, which is fed by the 1255 keV level via a 209 keV transition not shown in the figure. (c) A triton energy spectrum in coincidence with the 922 keV γ ray. The narrow peak corresponds to direct population of the 1255 keV level. In contrast to the 2_1^+ to ground-state transition, notice that for this nonyrast level there is comparatively little feeding from higher-lying excited sates.

The levels and γ rays observed in ^{150,152}Sm are listed in Tables I and II, respectively. Numerous new levels and γ-ray-emitting transitions were identified. In the first two columns the level energy and γ-ray energies are listed. The relative γ-ray branching for each level, expressed as a percentage of the strongest transition, is listed in the third

TABLE I. Levels and γ rays observed in the ^{152}Sm(p,t) reaction. Refer to the text for the full description of each column. The uncertainties are indicated by the superscript. Newly identified levels and γ rays are shown in bold. A dash in columns 4 and 5 indicates that the triton peak corresponding to the direct population of the level was not measured in coincidence with the γ ray in this row. This tends to occur for levels that are strongly fed by higher-lying states. In this case, a γ ray may still be placed if there are multiple observed transitions depopulating the level, or if it is a well-known transition from a low-lying state.

E_x (keV)	E_γ (keV)	I_γ	E_x^t (keV)	$E_x^t - E_\gamma$ (keV)	E_f^{ND} (keV)	$E_\gamma + E_f^{ND}$ (keV)	$J^{\pi,ND}$	E_x^{ND} (keV)	E_γ^{ND} (keV)	I_γ^{ND}	$\sigma_{(34^\circ-58^\circ)}$ (% of 2_1^+)
333.7^{2}	333.7^{2}	100	341^{14}	7^{14}	0	333.7^{2}	2^+	333.955^{10}	333.961^{11}	100^{3}	100^{2}
740.6^{2}	406.6^{2}	100	741^{4}	334^{4}	333.96	740.6^{2}	0^+	740.464^{19}	406.508^{22}	100	282^{6}
773.3^{3}	439.3^{3}	100	780^{5}	341^{5}	333.96	773.3^{3}	4^+	773.374^{12}	439.400^{14}	100	9.7^{8}
1046.3^{2}	712.4^{3}	100	1054^{11}	342^{11}	333.96	1046.4^{3}	2^+	1046.148^{13}	712.207^{14}	100^{6}	32^{2}
	1046.2^{2}	6^{2}	1031^{13}	-15^{13}	0	1046.2^{2}			1046.16^{14}	8.1^{9}	
1071.7^{2}	297.5^{5}	8^{2}	–	–	773.37	1070.9^{5}	3^-	1071.406^{12}	298.060^{13}	6.70^{23}	22^{2}
	737.7^{2}	100	1070^{5}	332^{5}	333.96	1071.7^{2}			737.457^{15}	100.0^{19}	
1165.6^{2}	831.6^{3}	84^{5}	–	–	333.96	1165.6^{3}	1^-	1165.791^{17}	831.83^{5}	75^{3}	–
	1165.5^{3}	100	–	–	0	1165.5^{3}			1165.74^{3}	100^{4}	
1193.9^{2}	860.0^{3}	67^{5}	1193^{5}	332^{5}	333.96	1194.0^{3}	2^+	1193.843^{12}	859.88^{3}	73.3^{16}	38^{2}
	1193.8^{2}	100	1194^{4}	0^{4}	0	1193.8^{2}			1193.830^{22}	100^{3}	
1255.4^{1}	209.2^{2}	11^{1}	1258^{4}	1049^{4}	1046.15	1255.3^{2}	0^+	1255.512^{20}	209.364^{19}	8.9^{16}	186^{4}
	921.5^{2}	100	1259^{4}	338^{4}	333.96	1255.5^{2}			921.55^{13}	100^{7}	
1278.9^{2}	505.5^{2}	100	1271^{7}	766^{7}	773.37	1278.9^{2}	6^+	1278.922^{14}	505.508^{23}	100	5.5^{6}
1357.9^{4}	584.5^{4}	100	1365^{7}	781^{7}	773.37	1357.9^{4}	5^-	1357.710^{13}	584.274^{12}	100^{3}	6^{1}
1417.2^{2}	251.2^{4}	48^{5}	1418^{5}	1167^{5}	1165.74	1417.0^{4}	2^+	1417.346^{13}	251.582^{19}	43.7^{18}	30^{2}
	345.8^{3}	100	1417^{4}	1071^{4}	1071.41	1417.2^{3}			345.950^{17}	100^{10}	
	1083.3^{3}	30^{5}	1427^{10}	344^{10}	333.96	1417.3^{3}			1083.34^{4}	70^{8}	
1449.7^{4}	676.3^{4}	100	1454^{12}	778^{12}	773.37	1449.7^{4}	4^+	1449.182^{13}	675.853^{24}	100^{2}	2.3^{6}
1505.2^{6}	1171.2^{6}	100	–	–	333.96	1505.2^{6}	3^+	1504.572^{13}	1170.589^{24}	100.0^{14}	–
1603.1^{7}	**1269.1^{7}**	100	1610^{40}	341^{40}	333.96	1603.1^{7}		1603^{4}			1.1^{4}
1642.6^{7}	869.2^{7}	100	1638^{22}	769^{22}	773.37	1642.6^{7}	4^+	1642.611^{12}	869.256^{14}	100^{1}	2.0^{5}
1684.1^{3}	911.0^{6}	60^{7}	1715^{27}	804^{27}	773.37	1684.4^{6}	3^-	1684.162^{17}	910.88^{4}	50^{6}	3.5^{6}
	1349.9^{4}	100	1698^{20}	348^{20}	333.96	1683.9^{4}			1350.28^{10}	100^{6}	
1764.8^{3}	485.9^{3}	100	1783^{20}	1297^{20}	1278.92	1764.8^{3}	7^-	1764.89^{4}	485.8^{3}	100^{4}	1.1^{3}
1786.3^{5}	620.5^{5}	100	1778^{12}	1158^{12}	1165.79	1786.3^{5}	$(\leqslant 3)$	1786.30^{13}	620.40^{20}	95^{16}	1.8^{5}
1794.2^{2}	600.5^{4}	44^{8}	–	–	1193.84	1794.3^{4}	2^+	1794.30^{3}	600.43^{25}	15^{3}	13^{1}
	628.5^{3}	100	1796^{7}	1168^{7}	1165.79	1794.3^{3}			628.56^{14}		
	722.9^{4}	56^{10}	1802^{12}	1079^{12}	1071.41	1794.3^{4}			722.65^{18}	24^{4}	
	1459.9^{4}	42^{10}	1764^{16}	304^{16}	333.96	1793.9^{5}					
1819.9^{2}	748.5^{2}	100	1806^{12}	1058^{12}	1071.41	1819.9^{2}	4^+	1819.510^{13}	748.06^{9}	100^{2}	7.6^{9}
	1485.5^{6}	24^{8}	1828^{26}	343^{26}	333.96	1819.5^{6}			1485.50^{14}	36.7^{15}	
1826.7^{3}	**1053.3^{3}**	100	1824^{8}	771^{8}	773.37	1826.7^{3}					5.3^{7}
1832.8^{2}	667.3^{3}	48^{8}	1834^{10}	1167^{10}	1165.79	1833.1^{3}	$(2)^+$	1833.01^{3}	667.05^{3}	100^{4}	13^{1}
	1498.7^{2}	100	1832^{8}	333^{8}	333.96	1832.7^{2}			1499.35^{10}	15.2^{7}	
1836.9^{2}	558.1^{2}	100	–	–	1278.92	1836.9^{2}	8^+	1837.03^{10}	558.1^{1}	100	–
1950.2^{2}	1176.8^{2}	100	1960^{7}	783^{7}	773.37	1950.2^{2}	3^-	1952.46^{3}	1176.6^{13}	100^{20}	8.6^{9}
1962.9^{7}	1222.4^{7}	100	1948^{28}	726^{28}	740.46	1962.9^{7}	$1^{(-)}$	1963.72^{4}	1223.26^{8}	100^{7}	1.5^{5}
2004.8^{4}	811.2^{6}	45^{12}	2005^{14}	1194^{14}	1193.84	2005.0^{6}	2^+	2005.5^{8}	812.1^{8}		7^{1}
	2004.6^{5}	100	2008^{16}	3^{16}	0	2004.6^{5}					
2117.0^{4}	1343.6^{4}	100	2114^{12}	770^{12}	773.37	2117.0^{4}	4^+	2117.030^{15}	1343.78^{22}	100^{3}	4.9^{7}
2152.7^{4}	1379.3^{4}	100	2157^{17}	778^{17}	773.37	2152.7^{4}	4^+	2152.56^{3}	1379.12^{6}	100^{12}	4.3^{7}
2260.1^{3}	1926.1^{3}	100	2265^{9}	339^{9}	333.96	2260.1^{3}	(1^-)	2259.94^{4}	1926.04^{8}	33^{7}	11^{1}
2362.6^{2}	**1290.9^{3}**	66^{13}	2358^{8}	1067^{8}	1071.41	2362.3^{3}					13^{1}
	2028.9^{3}	100	2373^{12}	344^{12}	333.96	2362.9^{3}					
2587.2^{4}	**1813.8^{4}**	100	2602^{24}	773^{24}	773.37	2587.2^{4}	$3^+,4^+$	2587.3^{5}			4.3^{9}
2654.9^{7}	**2320.9^{7}**	100	2640^{22}	319^{22}	333.96	2654.9^{7}	(3,5)	2655^{7}			4.0^{9}
2715.5^{3}	**1521.7^{3}**	100	2734^{18}	1212^{18}	1193.84	2715.5^{3}	3^-	2715^{4}			5.5^{8}
3018.3^{6}	**1852.5^{6}**	100	3018^{12}	1166^{12}	1165.79	3018.3^{6}					4.3^{9}
3037.8^{9}	2702.9^{13}	100	3042^{8}	339^{8}	333.96	3036.9^{13}	$1,2^+$	3038.2^{4}	2704.6^{7}	100^{5}	40^{3}
	3038.5^{12}	30^{8}	3060^{18}	22^{18}	0	3038.5^{12}			3037.8^{10}	33^{17}	
3045.3^{15}	**2711.3^{15}**	100	3045^{9}	334^{9}	333.96	3045.3^{15}					38^{3}

TABLE II. Same as Table I but for the ^{154}Sm(p,t) reaction. Refer to the text for full description of each column. The uncertainties are indicated by the superscript. Newly identified levels and γ rays are shown in bold.

E_x (keV)	E_γ (keV)	I_γ	E_x^t (keV)	$E_x^t - E_\gamma$ (keV)	E_f^{ND} (keV)	$E_\gamma + E_f^{ND}$ (keV)	$J^{\pi,ND}$	E_x^{ND} (keV)	E_γ^{ND} (keV)	I_γ^{ND}	$\sigma_{(34^\circ-58^\circ)}$ (% of 2_1^+)
121.7^{2}	121.7^{2}	100	115^{8}	-7^{8}	0	121.7^{2}	2^+	121.7818^{3}	121.7817^{3}	100	100^{2}
366.2^{2}	244.4^{2}	100	364^{9}	119^{9}	121.78	366.2^{2}	4^+	366.4793^{9}	244.6974^{8}	100	8.0^{5}
685.2^{3}	563.4^{3}	100	681^{9}	118^{9}	121.78	685.2^{3}	0^+	684.751^{21}	562.98^{3}	100.0^{19}	95^{2}
706.7^{3}	340.2^{3}	100	704^{8}	364^{8}	366.48	706.7^{3}	6^+	706.928^{17}	340.45^{3}	100	6.5^{5}
810.6^{2}	443.7^{5}	36^{3}	812^{7}	368^{7}	366.48	810.2^{5}	2^+	810.453^{5}	444.00^{3}	34.8^{13}	47^{2}
	688.8^{2}	100	817^{8}	128^{8}	121.78	810.6^{3}			688.670^{5}	100.0^{6}	
	810.7^{4}	46^{4}	799^{7}	-12^{7}	0	810.7^{4}			810.451^{5}	37.0^{3}	
963.3^{3}	841.5^{2}	100	–	–	121.78	963.3^{3}	1^-	963.358^{5}	841.570^{5}	100.0^{18}	–
1023.1^{3}	656.5^{3}	100	1025^{12}	369^{12}	366.48	1023.0^{3}	4^+	1022.970^{5}	656.489^{5}	100.0^{15}	5.0^{7}
	901.6^{5}	69^{16}	1039^{14}	137^{14}	121.78	1023.4^{5}			901.19^{5}	59.2^{17}	
1041.2^{2}	674.7^{4}	27^{5}	1036^{12}	361^{12}	366.48	1041.1^{4}	3^-	1041.122^{4}	674.65^{3}	40.4^{8}	13^{1}
	919.5^{3}	100	1031^{8}	112^{8}	121.78	1041.3^{3}			919.337^{4}	100.0^{10}	
1085.6^{2}	963.7^{3}	100	1082^{8}	118^{8}	121.78	1085.5^{3}	2^+	1085.841^{5}	964.057^{5}	100.00^{24}	42^{2}
	1085.7^{3}	57^{5}	1089^{9}	3^{9}	0	1085.7^{3}			1085.837^{10}	69.71^{10}	
1125.3^{3}	418.4^{3}	100	–	–	706.93	1125.3^{3}	8^+	1125.39^{3}	418.45^{3}	100	–
1221.6^{3}	855.1^{3}	100	1214^{11}	359^{11}	366.48	1221.6^{3}	5^-	1221.64^{3}	855.21^{7}	100^{3}	3.5^{5}
1233.9^{2}	867.9^{4}	46^{8}	–	–	366.48	1234.4^{4}	3^+	1233.863^{3}	867.380^{3}	30.93^{18}	–
	1112.0^{2}	100	–	–	121.78	1233.8^{2}			1112.076^{3}	100.0^{5}	
1293.0^{14}	926.5^{14}	100	1276^{15}	350^{15}	366.48	1293.0^{14}	2^+	1292.773^{10}	926.29^{4}	100.0^{12}	2.2^{5}
1310.5^{3}	603.6^{3}	100	–	–	706.93	1310.5^{3}	6^+	1310.505^{22}	603.56^{3}	100^{4}	–
1371.7^{3}	1005.2^{6}	100	1393^{22}	388^{22}	366.48	1371.7^{3}	4^+	1371.735^{12}	1005.27^{5}	100.0^{16}	3.2^{5}
1505.9^{3}	799.0^{3}	100	–	–	706.93	1505.9^{3}	7^-	1505.77^{3}	798.82^{3}	100^{3}	–
1510.9^{4}	1389.1^{4}	100	1542^{20}	153^{20}	121.78	1510.9^{4}	1^-	1510.790^{25}	1389.03^{4}	100.0^{21}	1.6^{5}
1559.6^{3}	1193.1^{3}	100	–	–	366.48	1559.6^{3}	5^+	1559.62^{3}	1193.10^{5}	100^{3}	–
1579.4^{2}	1212.9^{2}	100	1577^{9}	364^{9}	366.48	1579.4^{2}	3^-	1579.429^{11}	1212.948^{11}	100.0^{4}	8^{1}
	1457.4^{4}	42^{10}	1574^{18}	117^{18}	121.78	1579.2^{4}			1457.643^{11}	35.13^{26}	
1609.0^{4}	483.6^{4}	100	–	–	1125.39	1609.0^{4}	10^+	1609.26^{4}	483.86^{3}	100	–
1613.8^{4}	906.9^{4}	100	1618^{16}	711^{16}	706.93	1613.8^{4}	4^+	1612.90^{4}	906.06^{10}	100^{5}	1.4^{4}
1659.8^{3}	696.4^{3}	100	1680^{12}	984^{12}	963.36	1659.8^{3}	0^+	1658.80^{25}	695.9^{3}	100^{5}	7^{1}
1728.2^{5}	1021.3^{5}	100	–	–	706.93	1728.2^{5}	6^+	1728.27^{3}	1021.41^{4}	100^{3}	–
1755.1^{2}	791.7^{2}	100	1772^{12}	980^{12}	963.36	1755.1^{2}	0^+	1754.98^{4}	791.67^{7}	100^{5}	9.8^{8}
1764.3^{3}	1057.2^{5}	68^{20}	1764^{19}	707^{19}	706.93	1764.1^{5}	5^-	1764.32^{5}	1057.36^{6}	100^{6}	3.2^{7}
	1398.0^{4}	100	1775^{18}	377^{18}	366.48	1764.5^{4}			1397.88^{7}	82^{5}	
1769.0^{1}	397.5^{5}	5^{2}	–	–	1371.74	1769.2^{5}	2^+	1769.132^{23}	397.75^{26}	1.9^{3}	141^{5}
	535.2^{3}	12^{2}	1796^{8}	1261^{8}	1233.86	1769.1^{3}			535.44^{12}	8.8^{7}	
	683.9^{8}	25^{3}	–	–	1085.84	1769.7^{8}			683.25^{9}	24.1^{14}	
	728.3^{5}	58^{6}	1773^{4}	1045^{4}	1041.12	1769.4^{5}			728.03^{4}	56.5^{19}	
	805.5^{6}	68^{6}	1760^{8}	955^{8}	963.36	1768.9^{6}			805.71^{9}	77^{3}	
	958.5^{3}	100	1777^{4}	819^{4}	810.45	1769.0^{3}			958.63^{5}	100^{6}	
	1084.5^{2}	79^{6}	–	–	684.75	1769.3^{2}			1084.36^{14}	54^{4}	
	1646.7^{3}	36^{5}	1781^{9}	134^{9}	121.78	1768.5^{3}			1647.44^{12}	36.9^{18}	
	1768.9^{2}	68^{8}	1779^{8}	10^{8}	0	1768.9^{2}			1769.09^{5}	47.3^{11}	
1879.5^{3}	754.1^{3}	100	–	–	1125.39	1879.5^{3}	9^-	1879.14^{4}	753.83^{3}	100^{3}	–
1891.9^{4}	928.5^{4}	100	1899^{5}	971^{5}	963.36	1891.9^{4}	$0^+,1,2$	1892.48^{5}	929.12^{5}	100^{10}	21^{1}
1906.0^{2}	821.6^{11}	27^{12}	1910^{12}	1088^{12}	1085.84	1907.4^{11}	2^+	1906.13^{3}	820.31^{7}		29^{2}
	942.4^{3}	51^{12}	1890^{10}	948^{10}	963.36	1905.8^{3}			942.85^{6}	8.5^{12}	
	1784.5^{3}	100	1923^{13}	139^{13}	121.78	1906.3^{3}			1784.27^{7}	100^{8}	
	1905.9^{3}	96^{20}	1911^{10}	5^{10}	0	1905.9^{3}			1906.14^{7}		
1954.5^{7}	913.4^{7}	100	1940^{12}	1027^{12}	1041.12	1954.5^{7}	$3^-,4,5^-$	1954.30^{5}	913.17^{6}	100^{5}	2.8^{5}
2003.5^{6}	**1296.6^{6}**	100	2010^{20}	713^{20}	706.93	2003.5^{6}					2.3^{5}
2011.1^{3}	1644.6^{3}	70^{10}	2022^{10}	377^{10}	366.48	2011.1^{3}	$2^+,3,4^+$	2011.84^{5}	1645.30^{10}	100^{9}	19^{2}
	1889.4^{6}	100	2010^{10}	121^{10}	121.78	2011.2^{6}			1889.95^{6}	50^{9}	
2091.1^{2}	1050.1^{3}	99^{29}	2092^{10}	1042^{10}	1041.12	2091.2^{3}	$1^-,2$	2091.21^{4}	1050.10^{5}	100^{7}	8^{1}
	1127.6^{3}	100	2095^{11}	967^{11}	963.36	2091.0^{3}			1127.84^{5}	82^{7}	
2138.0^{2}	1096.9^{2}	100	2138^{11}	1041^{11}	1041.12	2138.0^{2}	2^+	2138.17^{12}	1096.96^{12}	100^{4}	7^{2}
2138.5^{8}	2016.7^{8}	100	2120^{40}	103^{40}	121.78	2138.5^{8}	$(2^+,3,4^+)$	2137.92^{6}	2016.17^{7}		2.3^{7}

TABLE II. (*Continued.*)

E_x (keV)	E_γ (keV)	I_γ	E_x^t (keV)	$E_x^t - E_\gamma$ (keV)	E_f^{ND} (keV)	$E_\gamma + E_f^{ND}$ (keV)	$J^{\pi,ND}$	E_x^{ND} (keV)	E_γ^{ND} (keV)	I_γ^{ND}	$\sigma_{(34^\circ-58^\circ)}$ (% of 2_1^+)
2214.9^{8}	**2093.1^{8}**	100	2202^{26}	109^{26}	121.78	2214.9^{8}					6^{1}
2246.1^{2}	**1160.3^{3}**	100	2249^{6}	1089^{6}	1085.84	2246.1^{3}					24^{2}
	1163.3^{4}	77^{24}	2245^{8}	1082^{8}	1082.84	2246.1^{4}					
	2245.8^{8}	41^{12}	2234^{24}	-15^{24}	0	2245.8^{8}					
2247.0^{2}	**1283.9^{4}**	100	2249^{8}	965^{8}	963.36	2247.3^{4}					14^{1}
	2125.1^{3}	95^{28}	2262^{18}	137^{18}	121.78	2246.9^{3}					
2285.2^{3}	1321.8^{3}	100	2296^{30}	974^{30}	963.36	2285.2^{3}	0,1,2	2284.96^{20}	1321.6^{2}		6.3^{8}
2320.5^{2}	516.9^{3}	100	2323^{9}	1806^{9}	1803.94	2320.8^{3}	4^+,5	2320.35^{23}	516.3^{4}	100^{10}	47^{3}
	1613.2^{4}	9^{3}	2288^{19}	675^{19}	706.93	2320.1^{4}			1613.4^{6}	13^{3}	
	1953.8^{3}	29^{5}	2324^{10}	370^{10}	366.48	2320.3^{3}			1953.7^{4}	30^{7}	
2331.1^{4}	**1624.2^{4}**	100	2348^{18}	724^{18}	706.93	2331.1^{4}					6.4^{9}
2365.4^{3}	**1998.9^{3}**	100	2369^{13}	370^{13}	366.48	2365.4^{3}					8^{1}
2462.7^{5}	**1499.3^{5}**	100	2456^{12}	957^{12}	963.36	2462.7^{5}					3.5^{6}
2567.8^{7}	2201.3^{7}	100	2566^{20}	365^{20}	366.48	2567.8^{7}	4^+,5	2567.06^{17}	2200.7^{2}	100^{17}	3.1^{9}
2705.0^{8}	**2583.2^{8}**	100	2702^{11}	119^{11}	121.78	2705.0^{8}					5^{1}
3039.1^{8}	**2917.3^{8}**	100	3038^{18}	121^{18}	121.78	3039.1^{8}					7^{2}
3132.0^{5}	**2765.5^{5}**	100	3134^{12}	369^{12}	366.48	3132.0^{5}					9^{3}

column. In column four the triton peak energy from the present work is listed, which is obtained from fitting the peak corresponding to direct population of the level after gating on the γ ray from the same row of the table. In the fifth column the γ-ray energy is subtracted from the triton peak energy. This can be compared with the corresponding level energy from the database of the National Nuclear Data Center at Brookhaven National Laboratory (NNDC) [16] listed in the sixth column. For a definite assignment to be made, we require that these values lie within one standard deviation of each other. In the seventh column the γ-ray energy obtained in the present work is summed with the NNDC energy from column six to obtain the precise level energy. For levels which decay by multiple observed γ rays, the final level energy was obtained from a weighted average of the values in column seven.

In columns eight to eleven the spin and parity, excitation energy, γ-ray energy, and relative γ-ray branching from the NNDC database are listed for previously known levels to compare with the values obtained in the present work. The NNDC values for γ-ray energies and intensities are only listed for γ rays observed in the present work; the full set of known γ rays for each level can be found in Ref. [16].

Figures 5 and 6 show the primary γ-ray decays observed from levels directly populated in the region of the PLS for ^{150}Sm and ^{152}Sm, respectively. Newly identified levels and newly identified or newly placed γ-ray transitions are shown in red, and the region of the PLS is indicated by the dashed lines. In Figs. 7 and 8, excitation energy is plotted against spin for levels directly populated in the present work. Newly identified levels are shown in red. The horizontal lines indicate possible spin ranges for the levels based on the spins of the levels populated by their γ decay.

In the following sections the levels populated in ^{150}Sm and ^{152}Sm in the present work are discussed. Comments are provided only for levels for which new information was obtained or when required for a full understanding of the results presented in Tables I and II.

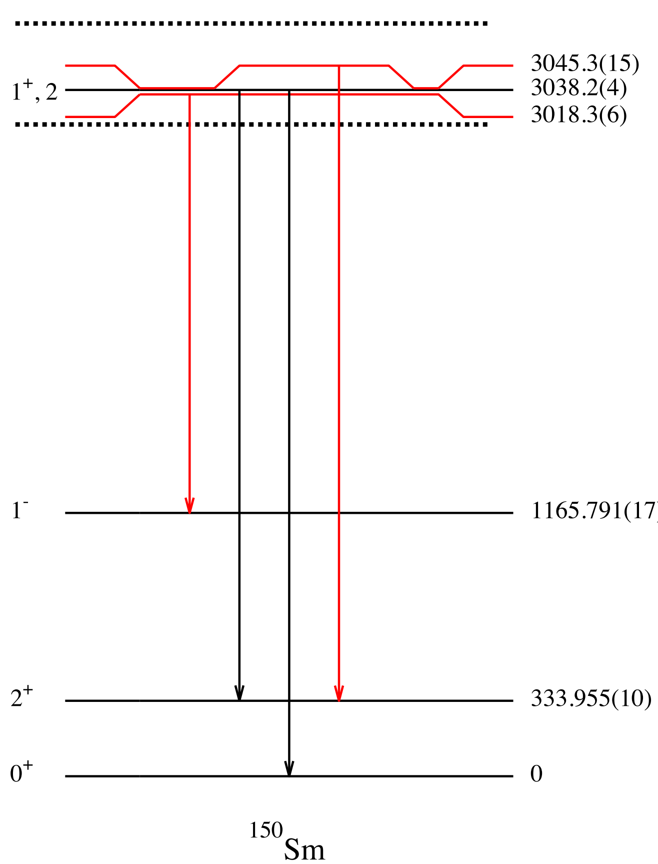

FIG. 5. Partial level scheme of ^{150}Sm showing the primary γ-ray decays from levels directly populated in the ^{152}Sm(p,t) reaction, in the region of the PLS indicated by the dashed lines. Newly identified levels and γ rays are shown in red.

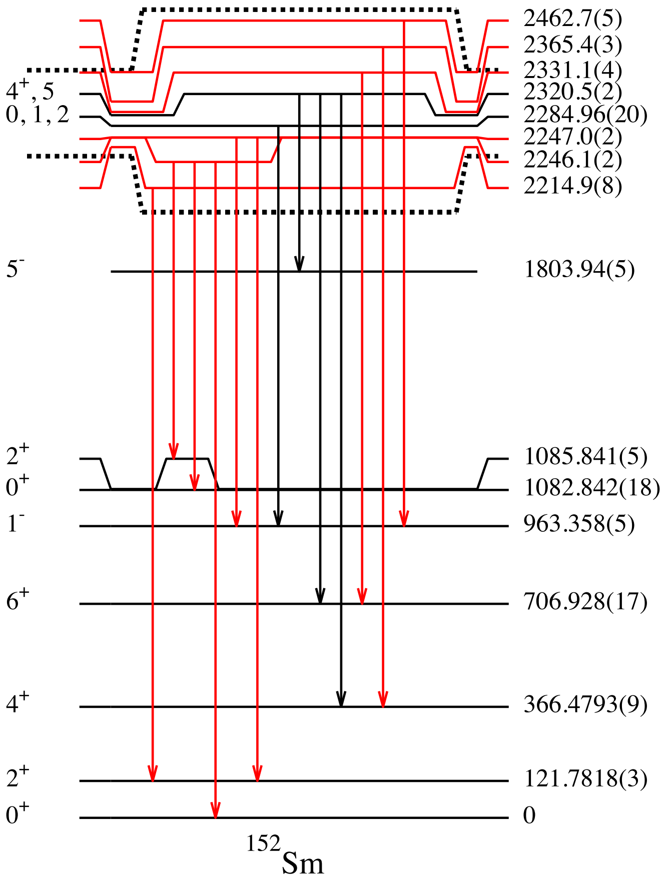

FIG. 6. Same as Fig. 5 but for ^{152}Sm from the ^{154}Sm(p,t) reaction.

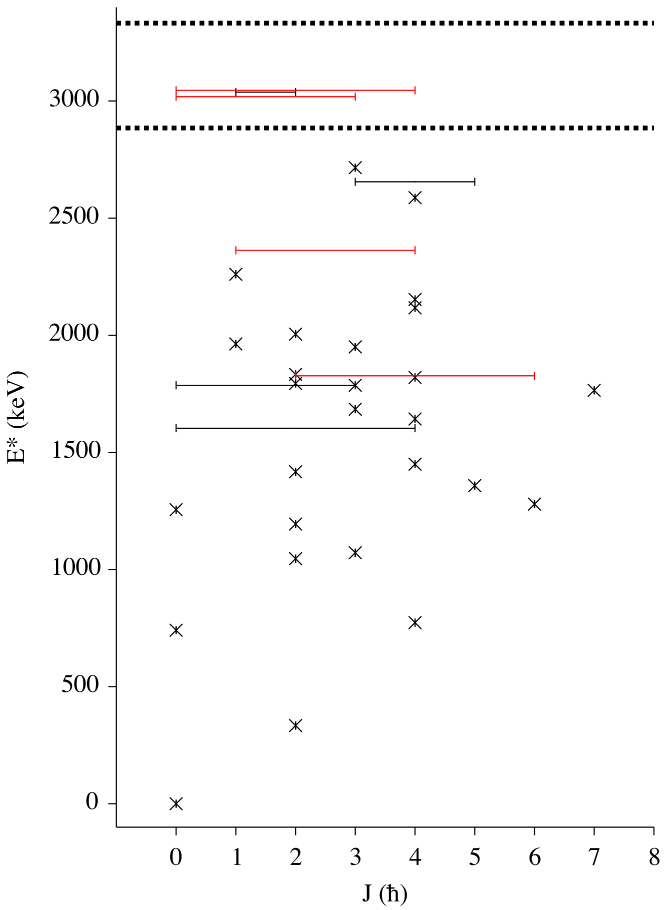

FIG. 7. A plot of excitation energy against spin for levels directly populated in ^{150}Sm. States of known spin are indicated by a black cross. Newly observed states are shown in red. States for which the spin is uncertain are plotted as horizontal lines. The range of possible spins for each level was obtained either from the literature, when available, or estimated by using the observed primary γ-ray transitions by assuming that the spin of a level was within two units of angular momentum of the states it was observed to feed. The region of the PLS is indicated by the black dashed lines.

A. Comments on levels and γ-ray transitions observed in ^{150}Sm

1. *The level at 1603.1(7) keV*

A 1269.1(7) keV γ-ray transition was placed between the 1603.1(7) keV and 2_1^+ levels. The cross section for the population of this level was measured by Debenham to be 0.48% of the cross section for populating the 0_2^+ level, with both measurements at a laboratory angle of 25 degrees. This is consistent with the value of 0.39(14)% obtained in the present work, integrated across the entire angular range of the telescope, and including only the strength decaying via the 1269.1(7) keV γ ray.

2. *The level at 1794.2(2) keV*

The NNDC database lists a 2^+ state at 1794.30(3) keV with four known γ rays at energies of 151.64(4), 600.43(25), 722.65(18), and 1798(4) keV. In the present work, the 1798(4) keV γ ray was not observed; it should be seen in the spectrum if the relative intensity from the literature is correct, and it is likely that this transition was misassigned. The 151.64(4) transition was also not observed, but would not be expected to be seen in the spectrum due to the low relative intensity. In addition, we assign to this level 628.5(3) and 1459.9(4) keV transitions.

3. *The level at 1826.7(3) keV*

A 1053.3(3) keV γ ray is newly observed in prompt coincidence with a state populated at 1824(8) keV in the particle data. This transition is assigned between a new level at 1826.7(3) keV and the 4^+ state at 773.374(12) keV. However, there are insufficient statistics to confirm this assignment by using t-γ-γ coincidences. Thus, the assignment of this level remains tentative.

4. *The level at 1832.8(2) keV*

The NNDC database lists a level at 1833.01 keV with four γ-ray transitions at energies of 667.05(3), 788, 1499.35(10), and 1833.30(15) keV. The 667.05(3) keV γ ray is listed as the strongest transition, which is in disagreement with the current work where it is observed to have 48(8)% of the strength of a 1498.7(2) keV transition. However, the 667.05(3) keV

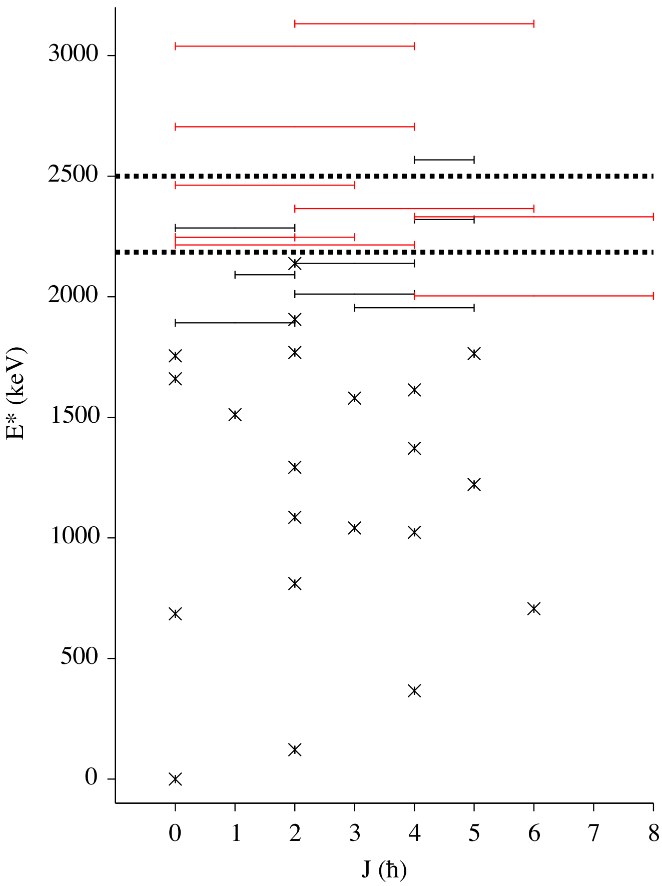

FIG. 8. Same as Fig. 7 but for ^{152}Sm.

transition is multiply placed in the NNDC database and the undivided intensity is given, which explains this discrepancy.

5. The level at 1950.2(2) keV

A 1176.8(2) keV transition is observed from the level at 1950.2(2) keV. The NNDC database makes a tentative assignment of a second γ-ray transition at 308.05(4) keV. However, energy of the state obtained in the present work is not consistent with this second transition. Therefore, we cannot confirm the assignment of the 308 keV γ ray to this level.

6. The level at 2260.1(3) keV

A level at 2260.1(3) keV is identified based upon a 1926.1(3) keV transition to the 2_1^+ level. Barrette *et al.* [21] reported a level at 2259.8 keV with eight decays, including a 1926.04(8) keV transition. Based upon our nonobservation of the other seven γ rays reported in Ref. [21], it seems likely that multiple discrete states occur near 2260 keV, of which only the 2260.1(3) keV level is observed in the present work.

7. The level at 2362.6(2) keV

A new level is observed at an excitation energy of 2362.6(2) keV with the two γ-ray transitions of 1290.9(3) and 2028.9(3) keV. The triton energy spectra gated on these two γ rays are shown in Fig. 9, where the level energy obtained by summing

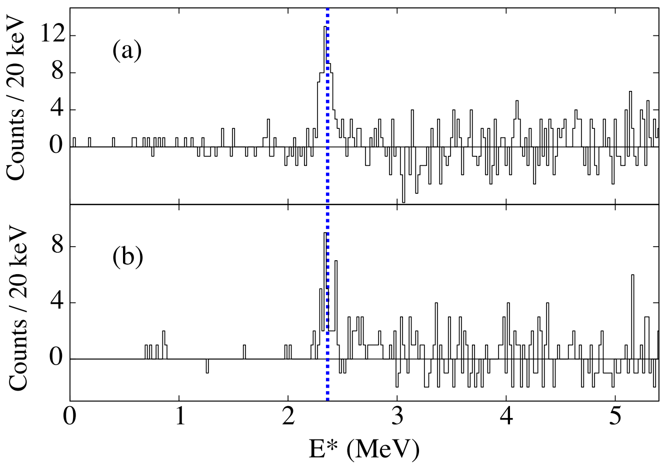

FIG. 9. Triton energy spectra obtained by gating on (a) the 1290.9(3) keV and (b) the 2028.9(3) keV γ rays, showing peaks measured at 2358(8) and 2373(12) keV, respectively. The blue dashed line indicates the excitation energy of 2362.6(2) keV obtained by summing the γ-ray energies with the NNDC energies of the lower-lying levels.

the γ-ray energies with the NNDC energies of the lower-lying levels is indicated by the blue dashed line.

8. The level at 2587.2(4) keV

A new 1813.8(4) keV γ-ray transition is observed between the level at 2587.2(4) keV and the 4_1^+ state, consistent with the previous measurements of the energy of this level [22,23]. This level is likely to be a 4^+ state based on the previous 3^+, 4^+ assignment from Ref. [23] and the natural-parity selection rule in the (p,t) reaction.

9. The level at 2654.9(7) keV

A 2320.9(7) keV transition is observed between the level at 2654.9(7) keV and the 2_1^+ state. It is possible that this is the NNDC level at 2655(7) keV [8,22,24,25]. A spin and parity of $3^{(+)}$, $5^{(+)}$ was previously assigned to this level [25], suggesting that the level is a 3^- state based on the transition to the 2_1^+ state and the natural-parity selection rule.

B. Comments on levels and γ-ray transitions observed in ^{152}Sm

1. The level at 2003.5(6) keV

A level is observed at an excitation energy of 2003.5(6) keV with a 1296.6(6) keV γ-ray transition. This state could correspond to one of three levels from the NNDC database at excitation energies of 2003.66(20), 2004.24(6), and 2004.29(11) keV. The latter two levels have known γ rays at energies of 1297.4(10) and 1297.29(13) keV, respectively.

2. The level at 2214.9(8) keV

A new 2093.1(8) keV γ ray from the level at 2214.9(8) keV is observed. A level has previously been observed at an excitation energy of 2214.92(10) keV [26]. However, this level has been assigned as a 8^+ state which is inconsistent with the transition to the 2_1^+ state observed in the present work.

3. The levels at 2246.1(2) and 2247.0(2) keV

A level at 2246.1(2) keV is observed with three γ-ray transitions at energies of 1160.3(3), 1163.3(4), and 2245.8(8) keV. Additionally, a level at 2247.0(2) keV with two γ-ray transitions of 1283.9(4) and 2125.1(3) keV is observed. Separate level assignments are made since the level energies obtained by using the 1283.9(4) and 2125.1(3) keV transitions are 3.0 and 2.7 standard deviations, respectively, from the level energy evaluated by using the remaining three γ rays. A level at 2247.23 keV was previously observed [27] with transitions to the 0_1^+, 2_1^+, and 1_1^- levels.

4. The level at 2331.1(4) keV

A 1624.2(4) keV γ ray is observed and assigned as a transition to the 6_1^+ state from the level at 2331.1(4) keV. We note that a level at 2332.42 keV has been previously observed [27] in the $(\alpha,2n\gamma)$ reaction with transitions to the 6_1^+ and 8_1^+ levels.

5. The level at 2365.4(3) keV

A 1998.9(3) keV transition between the level at 2365.4(3) keV to the 4_1^+ level is observed. A level at 2365 keV has been previously observed [27] in the Coulomb excitation reaction with transitions to the 4^+ levels at 1371.735(12) and 1612.90(4) keV. These transitions, at 994 and 753 keV, respectively, are not observed in the present work despite the higher γ-ray detection efficiency at those energies. Therefore, it is unlikely that this is the same level.

6. The level at 2462.7(5) keV

A 1499.3(5) keV γ ray from a level at 2462.7(5) keV is observed. A 1498.7(2) keV γ ray is also observed in the ^{152}Sm(p,t) reaction, but the amount of contamination is expected to negligible. A level at 2463.17 keV was previously observed [27] in the $(n,n'\gamma)$ reaction with a transition to the 1_1^- state, which is consistent with the assignment made in the present work.

7. The level at 3132.0(5) keV

A new level is placed at an excitation energy of 3132.0(5) keV with a 2765.5(5) keV γ ray. The triton peak obtained by gating on this γ ray is shown in Fig. 10 and compared with the level energy obtained by summing the γ-ray energy with the NNDC energy of the lower-lying level.

IV. PARTIAL CROSS SECTIONS

Relative partial cross sections for the direct population of states in ^{150,152}Sm via the (p,t) reaction were obtained by gating on the γ rays listed in Tables I and II and measuring the area of the triton peak corresponding to the direct population of a level. We accounted for the γ-ray detection efficiency and, when possible, the internal conversion coefficient for the γ-ray transition. The missing strength due to unobserved γ rays and the finite angular coverage of the Si telescope were not corrected for and therefore these values should be considered as partial cross sections, averaged over the angular range of the telescope of 34 to 58 degrees. The values are given as a percentage of the cross section for direct population of the 2_1^+ level. The relative partial cross sections are listed in Tables I and II and plotted in Figs. 11 and 12 where they are compared with the triton projections of the t-γ coincidence matrices for the ^{152}Sm(p,t) and ^{154}Sm(p,t) reactions, respectively. Overall the correspondence between the two is very good.

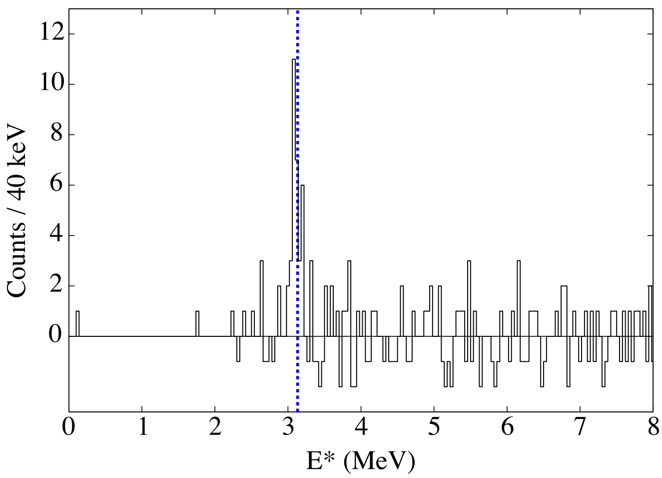

FIG. 10. Triton energy spectrum obtained by gating on the 2765.5(5) keV γ ray. The dashed blue line indicates the level energy obtained by summing the γ-ray energy with the NNDC energy of the lower-lying level that is fed.

Cross sections for populating excited states in ^{150,152}Sm via the (p,t) reaction have previously been measured in Refs. [9–12]. In Table III the relative cross sections obtained in the present work for the ^{152}Sm(p,t) reaction are compared with those obtained by Debenham *et al.* [11] and McLatchie *et al.* [10]. Since the cross sections obtained in the present work are angle averaged between 34 to 58 degrees whereas the values quoted by Debenham are the maximum differential cross sections at the listed angle, this table is provided as

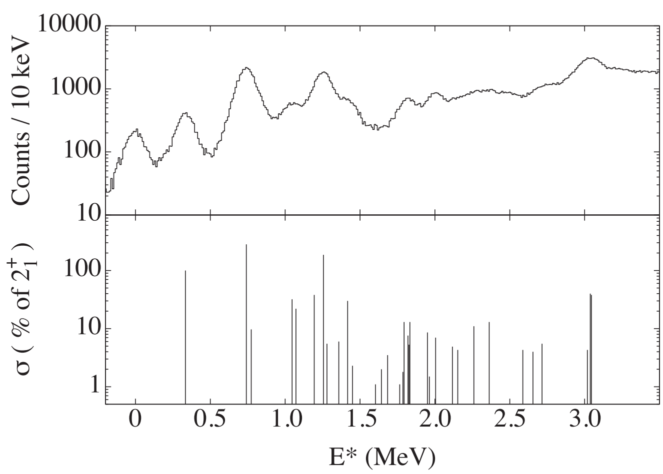

FIG. 11. (top) The triton energy projection from the ^{152}Sm(p,tγ) coincidence matrix. (bottom) The relative partial cross sections from Table I are plotted.

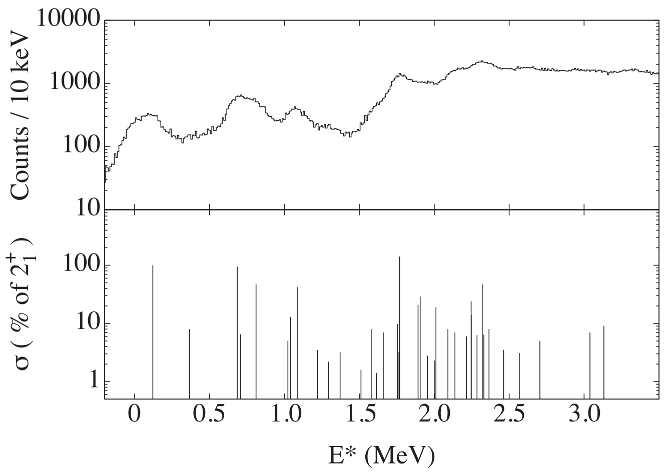

FIG. 12. Same as Fig. 11 but for the ^{154}Sm(p,t) reaction.

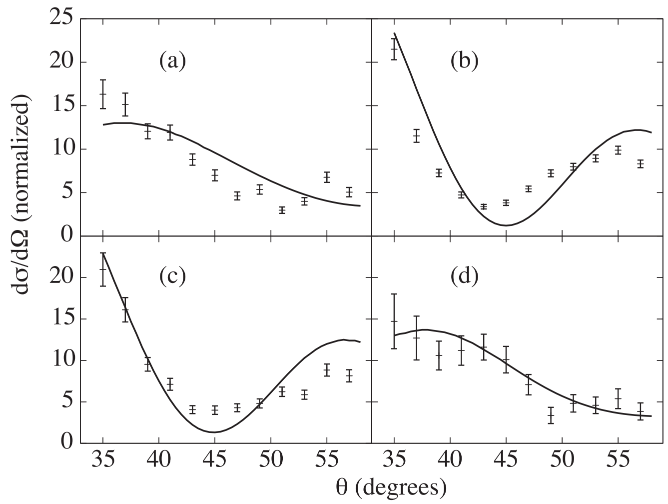

FIG. 13. Experimental angular distributions (black points with error bars) obtained by gating on primary γ rays from the levels populated in the ^{152}Sm(p,t) reaction at (a) 334 keV, $J = 2$ (b) 740 keV, $J = 0$ (c) 1256 keV, $J = 0$, and (d) 1417 keV, $J = 2$ are compared with DWBA calculations for $L = 0$ and 2 transfer (solid lines).

a general comparison only. It should be reemphasized that the values quoted in the present work are lower limits of the relative cross section if there are unobserved γ-ray decay branches. An incident proton energy of 19 MeV was used by Debenham. McLatchie quotes the differential cross section at 22.5° and used an incident proton energy of 20.6 MeV.

Overall, the agreement between the three data sets is good. It can be seen that the excited 0^+ states at 740.6(2) and 1255.4(1) keV have particularly large cross sections in all three sets of measurements. This has been interpreted in terms of shape coexistence and the rapid onset of deformation that occurs in this region [7,28].

TABLE III. The relative partial cross sections for levels in ^{150}Sm obtained in the present work are compared with the cross sections obtained by Debenham [11] and McLatchie [10]. The value reported by Debenham is the maximum differential cross section at the angle listed in the following column. All values are quoted relative to the 2_1^+ level at 333.7(2) keV, which has been scaled to 100. Debenham reports a relative error of 6.9%.

E_x (keV)	J^π	σ(34°–58°) Present work	$\sigma(\theta)_{max}$ Ref. [11]	θ (degrees)	σ(22.5°) Ref. [10]
333.7(2)	2^+	100(2)	100	10	100
740.6(2)	0^+	282(6)	260	25	340
773.3(3)	4^+	9.7(8)	9.9	10	<20
1046.3(2)	2^+	32(2)	42	10	<20
1071.7(2)	3^-	22(2)	5.6	35	40
1193.9(2)	2^+	38(2)	46	10	80
1255.4(1)	0^+	186(4)	170	25	180
1357.9(4)	5^-	6(1)	1.9	20	<20
1417.2(2)	2^+	30(2)	27	10	30
1449.7(4)	4^+	2.3(6)	3.7	12.5	<20
1603.1(7)		1.1(4)	1.2	25	
1642.6(7)	4^+	2.0(5)	1.2	10	
1794.2(2)	2^+	13(1)	17	10	
1832.8(2)	$(2)^+$	7.6(9)	6.8	20	<20
1950.2(2)	3^-	8.6(9)	3.7	35	<20

V. ANGULAR DISTRIBUTIONS

A. Discrete states

By measuring the angular distribution of the outgoing tritons, the orbital angular-momentum transfer can be determined by comparison to distributions obtained from DWBA calculations. For example, in Fig. 13 the experimental angular distributions from the population of the 334 (2^+), 740 (0^+), 1256 (0^+), and 1417 (2^+) keV levels are compared with DWBA calculations produced using the DWUCK4 code [29] for $L = 0$ and 2 transfer, respectively. The optical model potential used in the present work is defined in Ref. [30]. The proton potential from Ref. [30] was used and the triton and neutron parameters were obtained from Ref. [31]. These parameters are listed in Table IV. The experimental angular distributions were produced by gating on the primary γ-ray transitions from those levels, and measuring the angular distribution of the outgoing tritons in the Si telescope. For levels with multiple observed γ rays, the angular distributions obtained from each γ-ray gate were summed. It can be seen from Fig. 13 that the theoretical curves calculated assuming the NNDC J assignments are in good agreement with the experimental data.

The level at 2320 keV was previously assigned $J = 4^+$,5 in the NNDC database based on its γ-ray decay scheme. The angular distribution for this level is plotted in Fig. 14 where it is compared with the DWBA calculations for $L = 4$ and $L = 5$ transfer. The reduced χ^2 for the $L = 4$ and $L = 5$ curves are 2.1 and 2.2, respectively, therefore a definitive assignment cannot be made.

B. The peak-like structures

In Fig. 15(a), the angular distribution of the PLS observed in ^{150}Sm, centered at ~3 MeV, is compared with the angular distribution for the background under the PLS and with the

TABLE IV. Optical model parameters used in the DWBA calculations. The optical model potential used in the present work is defined in Ref. [30]. The proton parameters are from Ref. [30]. The triton and neutron parameters were obtained from Ref. [31].

	V_r (MeV)	W' (MeV)	W_0 (MeV)	V_{so} (MeV)	R_r (fm)	R_{is} (fm)	R_{iv} (fm)	R_{so} (fm)	a_r (fm)	a_{is} (fm)	a_{iv} (fm)	a_{so} (fm)	R_c (fm)	nlc[a]
p	57.5	29.6	3	5.65	1.200	1.150	1.259	1.010	0.670	0.779	0.76	0.75	1.25	0.85
t	160.03		17.83		1.200		1.400		0.720		0.84		1.30	0.25
n				$\lambda = 25$	1.17				0.75					

[a]Nonlocality parameter.

continuum region at higher excitation energy between 3.3 and 4 MeV. The error bars represent the statistical uncertainty only. The angular distribution for the PLS was obtained by measuring the strength built upon a smooth continuum background, illustrated in Fig. 16, for each ring-sector pixel of the Si telescope. The angular distribution for the background under the PLS was obtained from the area under the blue-shaded region, for each pixel. In Fig. 15(b) the angular distributions for the PLS and background in ^{152}Sm are similarly compared with the nearby continuum region between 2.5 and 3.0 MeV.

It can be seen in Figs. 15(a) and 15(b) that the angular distributions of the PLS are significantly different from the distributions obtained from the nearby continuum region, and that the angular distributions obtained for the background under the PLS are very similar to the distributions obtained for the continuum region. Figure 15(c) compares the angular distributions of the PLS observed in ^{150}Sm and ^{152}Sm. Despite the fact that the two PLS in the two nuclei are 700 keV apart in excitation energy, the two distributions are extremely similar. This suggests that the distributions of orbital angular-momentum transfers are similar in both reactions when populating the PLS. In Fig. 15(d) the angular distributions for the PLS are compared with the DWBA calculations which are most similar to the experimental data. The experimental distributions are most similar to the calculations for $L = 2$, 3, and 4 transfer, which are plotted as the blue, black, and red lines, respectively, calculated for the ^{152}Sm(p,t) reaction.

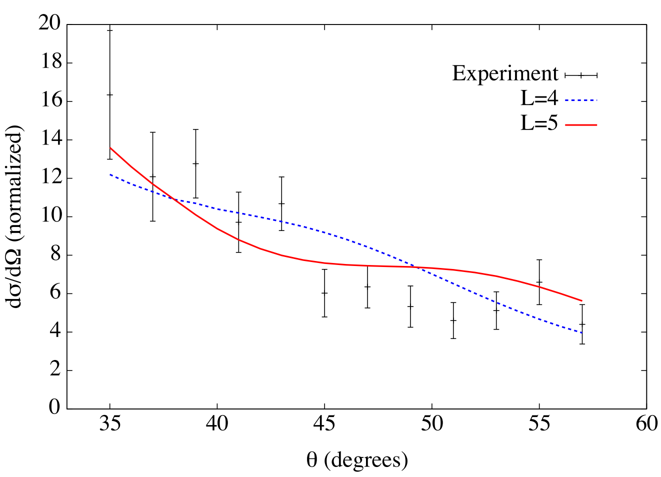

FIG. 14. The experimental angular distribution for the level at 2320.5(2) keV is compared with the DWBA calculations for $L = 4$ (dashed blue line) and $L = 5$ (solid red line) transfer.

VI. DISCUSSION AND SUMMARY OF RESULTS

Perhaps the most striking feature observed in the (p,t) spectra, Fig. 1, is the large PLS observed in all five Sm and Gd nuclei between 2–3 MeV excitation energy. There, a rapid increase in the triton intensity occurs and the smooth continuum "background" begins. Figure 2 shows that the energy of the PLS decreases with increasing neutron number, and that the structure is located at approximately the same excitation energy in Sm and Gd nuclei with the same neutron numbers. One hypothesis is that the structure is partially composed of states formed by the coupling of a neutron hole near the Fermi surface to a deep-lying neutron hole. Then, the energy of the structure is expected to decrease with increasing deformation, i.e., as one moves away from the $N = 82$ spherical shell gap. This deep-hole, valence-hole hypothesis has previously been suggested as an explanation for broad structures observed between 7–9 MeV in the ^{112,116,118,120,122,124}Sn(p,t) reactions [32]. Although it was initially suggested that these structures were formed by creating two deep-lying holes below the shell closure [33], it was found that the energy systematics were better described by the coupling of a valence hole to a deep hole [34]. It has also been shown in the review by Crawley [35] that bumps observed in two neutron-transfer reactions in the Cd isotopes are likely to correspond to a valence-hole deep-hole configuration. In the (p,t) study by Nakagawa *et al.* [36], bumps at lower and higher excitation energy, corresponding to valence-deep and deep-deep hole states, respectively, were observed across a wide range of nuclei from ^{66}Zn to ^{230}Th. This includes one isotope of samarium, ^{148}Sm, where a bump corresponding to the deep-deep configuration was observed at an excitation energy of approximately 6 MeV. The bump corresponding to the valence-deep configuration would be expected to lie at lower excitation energy. However, it must be noted that the FWHM of these structures in the $N = 82$ region is approximately 5 MeV, much larger than the narrow structures observed in the present work. A study of two-neutron hole strength in ^{142,146,148,150,152}Sm was performed by Struble *et al.* [13] where the broad structure observed by Nakagawa at 6 MeV in ^{148}Sm was also observed. The PLS observed in the present work can be seen in Fig. 4 of that paper labeled as peak *e*. It was suggested by Struble that these much narrower structures are associated with two-hole strength in strongly up-sloping orbitals from below the $N = 82$ shell closure.

In ^{152}Sm between 2.2 and 2.5 MeV, i.e., in the region of the PLS, a total of eight levels are found which are directly populated in the (p,t) reaction including six newly identified

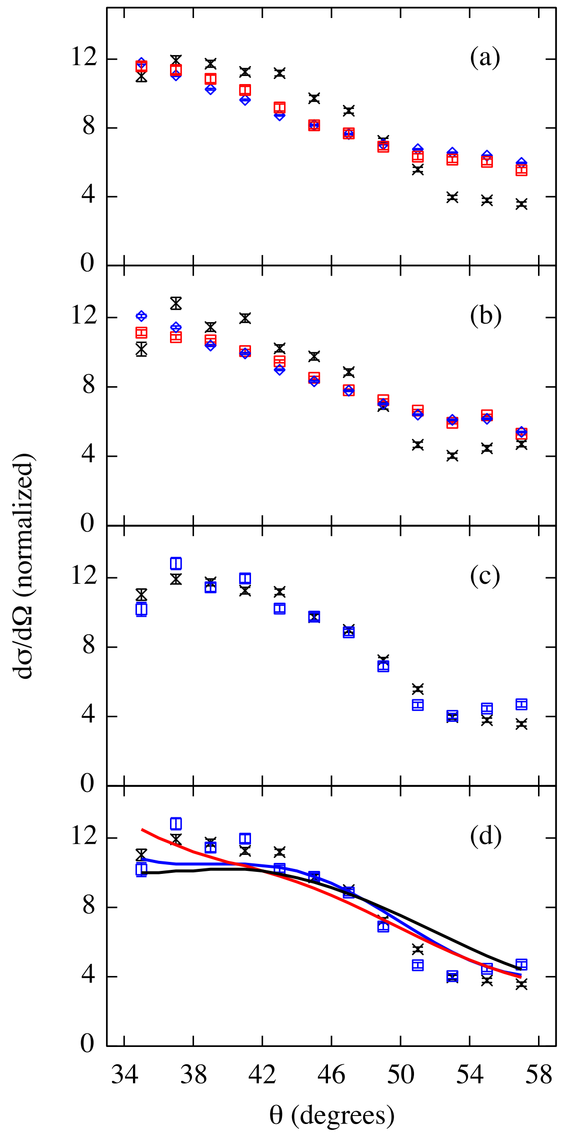

FIG. 15. (a) The angular distribution of the PLS in ^{150}Sm (black points) is compared with the angular distribution for the background under the PLS (red points) and the distribution obtained for the nearby continuum region between 3.3 and 4.0 MeV (blue points). (b) The angular distribution of the PLS in ^{152}Sm (black points) is compared with the angular distribution for the background under the PLS (red points) and the distribution obtained for the nearby continuum region between 2.5 and 3.0 MeV (blue points). (c) The angular distributions of the PLS observed in ^{150}Sm (black points) and ^{152}Sm (blue points) are compared. (d) Same as panel (c), except that the DWBA calculations for $L = 2$ (blue line), $L = 3$ (black line), and $L = 4$ (red line) transfer, calculated for the ^{152}Sm(p,t) reaction, are also plotted.

levels. The majority of likely spin values for these also range from 0 to 5$\hbar$. In ^{150}Sm the PLS is observed at a higher excitation energy, extending from 2.9 to 3.3 MeV. Only three discrete levels, including two newly identified ones, are observed in this energy region; see Fig. 5. This is due in part to the lower detection efficiency for higher-energy γ rays. Possible spin values for these levels lie in the 0–4$\hbar$ range; see Fig. 7.

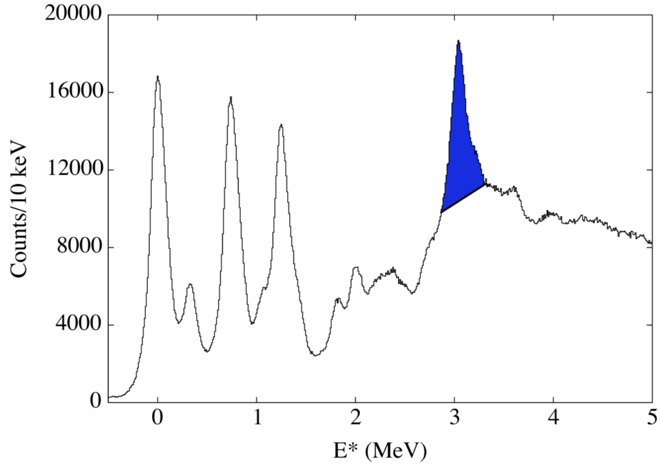

FIG. 16. The triton singles spectrum from the ^{152}Sm(p,t) reaction. The blue-shaded area corresponds to the counts considered to belong to the PLS when measuring the angular distributions shown in Fig. 15(c).

In ^{150}Sm, the relative cross section, within the angular range of the telescope, for the population of the PLS, and measured in the triton singles spectrum, is 213(20)% of the cross section for the direct population of the 2_1^+ level. Of this strength, 39(4)% can be accounted for by the discrete states observed in the present work. In ^{152}Sm, the strength of the PLS was observed to be be 117(19)% of the 2_1^+ level. Of this strength, 93(15)%, could be accounted for by the discrete states observed in the present work. This measurement is consistent with the spectrum seen in the top panel of Fig. 1 from Ref. [12]. There, it can be seen that the region of the PLS around 2.3 MeV in ^{152}Sm appears to be dominated by a relatively small number of states with large cross sections; in particular the level measured by Saha at an excitation energy of 2268 keV. This corresponds to the levels measured at 2246.1(2) and 2247.0(2) keV in the present work, because the excitation energies reported by Saha appear to be systematically too high.

The angular distributions of the PLS, shown in Fig. 15, differ significantly from that of the nearby continuum region and have a shape more characteristic of the single L-transfer curves. This suggests that the L-transfer distribution when populating the PLS is significantly different than when populating the adjacent continuum region, which supports the conclusion that the structures are dominated by a relatively low number of states of similar spins. The fact that the angular distributions of the PLS populated in the two reactions are very similar, as shown in Fig. 15(c), suggests that the L-transfer distributions are also similar.

In summary, numerous new levels and γ-ray transitions were identified in ^{150,152}Sm utilizing the t-γ coincidence technique, including in the region of the PLS observed between 2.3 and 3.0 MeV. These structures appear to be dominated by a relatively small number of discrete states, particularly in ^{152}Sm. The angular distributions of the outgoing tritons populating the PLS in the ^{152,154}Sm(p,t) reactions are very similar and significantly different from the angular distributions obtained by gating on the adjacent higher-excitation-energy continuum region.

ACKNOWLEDGMENTS

The authors are grateful to Professor J. L. Wood for information on levels and γ-ray transitions in ^{152}Sm and for helpful discussion of the data. This material is based on work supported by the U.S. Department of Energy, Office of Science, Office of Nuclear Physics under Grants No. DE-SC0014277, No. DE-FG02-05ER41379, and No. DE-FG02-93ER40773, by the U.S. Department of Energy, National Nuclear Security Administration under Grants No. DE-NA0002914, No. DE-NA0001801, and No. DE-FG52-09NA29467, by the National Science Foundation under contract PHY-130581, and by the U.S. Department of Energy NNSA Office of Defense Nuclear Nonproliferation Research & Development under Contract No. DE-AC52-07NA27344 (Lawrence Livermore National Laboratory).

[1] D. A. Meyer, V. Wood, R. F. Casten, C. R. Fitzpatrick, G. Graw, D. Bucurescu, J. Jolie, P. von Brentano, R. Hertenberger, H.-F. Wirth, N. Braun, T. Faestermann, S. Heinze, J. L. Jerke, R. Krücken, M. Mahgoub, O. Möller, D. Mücher, and C. Scholl, Phys. Rev. C **74**, 044309 (2006).

[2] N. V. Zamfir, J.-y. Zhang, and R. F. Casten, Phys. Rev. C **66**, 057303 (2002).

[3] D. Tonev, A. Dewald, T. Klug, P. Petkov, J. Jolie, A. Fitzler, O. Möller, S. Heinze, P. von Brentano, and R. F. Casten, Phys. Rev. C **69**, 034334 (2004).

[4] R. F. Casten, M. Wilhelm, E. Radermacher, N. V. Zamfir, and P. von Brentano, Phys. Rev. C **57**, R1553 (1998).

[5] F. Iachello, N. V. Zamfir, and R. F. Casten, Phys. Rev. Lett. **81**, 1191 (1998).

[6] P. E. Garrett, W. D. Kulp, J. L. Wood, D. Bandyopadhyay, S. Choudry, D. Dashdorj, S. R. Lesher, M. T. McEllistrem, M. Mynk, J. N. Orce, and S. W. Yates, Phys. Rev. Lett. **103**, 062501 (2009).

[7] J. R. Maxwell, G. M. Reynolds, and N. M. Hintz, Phys. Rev. **151**, 1000 (1966).

[8] J. H. Bjerregaard, O. Hansen, O. Nathan, and S. Hinds, Nucl. Phys. **86**, 145 (1966).

[9] W. Oelert, G. Lindström, and V. Riech, Nucl. Phys. A **233**, 237 (1974).

[10] W. McLatchie, W. Darcey, and J. E. Kitching, Nucl. Phys. A **159**, 615 (1970).

[11] P. Debenham and N. M. Hintz, Nucl. Phys. A **195**, 385 (1972).

[12] A. Saha, O. Scholten, D. C. J. M. Hageman, and H. Fortune, Phys. Lett. B **85**, 215 (1979).

[13] G. L. Struble, L. G. Mann, R. G. Lanier, W. M. Buckley, J. Kern, G. Crawley, S. Gales, D. Mueller, and F. Girshick, Phys. Rev. C **23**, 2447 (1981).

[14] H. J. Riezebos, R. De Leo, P. B. Goldhoorn, M. N. Harakeh, and L. W. Put, Phys. Lett. B **118**, 287 (1982).

[15] S. R. Lesher *et al.*, Nucl. Instrum. Methods Phys. Res., Sect. A **621**, 286 (2010).

[16] Evaluated Nuclear Structure Data File (ENSDF); National Nuclear Data Center (NNDC), Brookhaven National Laboratory (2014).

[17] Energy Loss and Straggling Tool (ELAST), adapted from the computer program ENELOSS, written by H. Ernst (1981) with stopping power routines by K. Lesko (1984).

[18] T. J. Ross, C. W. Beausang, R. O. Hughes, J. M. Allmond, C. T. Angell, M. S. Basunia, D. L. Bleuel, J. T. Harke, R. J. Casperson, J. E. Escher, P. Fallon, R. Hatarik, J. Munson, S. Paschalis, M. Petri, L. Phair, J. J. Ressler, N. D. Scielzo, and I. J. Thompson, Phys. Rev. C **85**, 051304(R) (2012).

[19] J. M. Allmond (unpublished).

[20] J. M. Allmond, C. W. Beausang, J. O. Rasmussen, T. J. Ross, M. S. Basunia, L. A. Bernstein, D. L. Bleuel, W. Brooks, N. Brown, J. T. Harke, B. K. Darakchieva, K. R. Dudziak, K. E. Evans, P. Fallon, H. B. Jeppesen, J. D. LeBlanc, S. R. Lesher, M. A. McMahan, D. A. Meyer, L. Phair, N. D. Scielzo, S. R. Stroberg, and M. Wiedeking, Phys. Rev. C **81**, 064316 (2010).

[21] J. Barrette, M. Barrette, S. Monaro, S. Santhanam, and S. Markiza, Can. J. Phys. **48**, 1161 (1970).

[22] L. V. Groshev, A. M. Demidov, V. A. Ivanov, V. N. Lutsenko, and V. I. Pelekhov, Nucl. Phys. **43**, 669 (1963).

[23] F. Bečvář, R. E. Chrien, and O. A. Wasson, Nucl. Phys. A **236**, 173 (1974).

[24] R. A. Kenefick and R. K. Sheline, Phys. Rev. **133**, B25 (1964).

[25] E. R. Reddingius and H. Postma, Nucl. Phys. A **137**, 389 (1969).

[26] J. Konijn *et al.*, Nucl. Phys. A **373**, 397 (1982).

[27] J. L Wood (private communication).

[28] T. Takemasa, M. Sakagami, and M. Sano, Phys. Lett. B **37**, 473 (1971).

[29] P. D. Kunz, DWUCK4 (University of Colorado, 1974).

[30] N. Blasi *et al.*, Nucl. Phys. A **624**, 433 (1997).

[31] H.-F. Wirth, G. Graw, S. Christen, D. Cutoiu, Y. Eisermann, C. Günther, R. Hertenberger, J. Jolie, A. I. Levon, O. Möller, G. Thiamova, P. Thirolf, D. Tonev, and N. V. Zamfir, Phys. Rev. C **69**, 044310 (2004).

[32] G. M. Crawley, W. Benenson, G. Bertsch, S. Gales, D. Weber, and B. Zwieglinski, Phys. Rev. C **23**, 589 (1981).

[33] G. M. Crawley, W. Benenson, D. Weber, and B. Zwieglinski, Phys. Rev. Lett. **39**, 1451 (1977).

[34] M. Nomura, Prog. Theor. Phys. **59**, 1771 (1978).

[35] G. M. Crawley, *Proc. 1980 RCNP International Symposium on Highly Excited States in Nuclear Reactions*, edited by H. Ikegami and M. Muraoka (Research Center for Nuclear Physics, Osaka University, Suita Osaka, Japan, 1980), p. 590.

[36] T. Nakagawa *et al.*, Nucl. Phys. A **376**, 513 (1982).